Sensing Copper (II) Ions with Hyper Rayleigh Scattering from Gold Nanoparticles

Krzysztof Nadolski, Fabien Rondepierre, Christian Jonin, Tomasz Marek Goszczyński, Katarzyna Matczyszyn, Pierre-François Brevet

Sensing Copper (II) Ions with Hyper Rayleigh Scattering from Gold Nanoparticles

Krzysztof Nadolski,[1,2] Fabien Rondepierre,[1] Christian Jonin,[1] Tomasz Marek Goszczyński,[3] Katarzyna Matczyszyn,[2] Pierre-François Brevet[1*]*

[1]Institut Lumière Matière, Université Claude Bernard Lyon 1, CNRS UMR 5306, 69100 Villeurbanne, France.

[2]Institute of Advanced Materials, Faculty of Chemistry, Wroclaw University of Science and Technology, 50-370 Wroclaw, Poland.

[3]Laboratory of Biomedical Chemistry, Hirszfeld Institute of Immunology and Experimental Therapy, Polish Academy of Sciences, 53-114 Wroclaw, Poland

KEYWORDS: gold nanoparticles, sensing, refractive index, nonlinear optics, hyper Rayleigh scattering

* Corresponding authors: Prof. Katarzyna Matczyszyn, katarzyna.matczyszyn@pwr.edu.pl; Prof. Pierre-François Brevet, pfbrevet@univ-lyon1.fr

ABSTRACT

Incoherent Second Harmonic Generation (SHG) from gold nanoparticles, also known as hyper-Rayleigh scattering (HRS), is proposed as a sensing method for copper (II) ions. As opposed to colorimetry based methods relying on the shift of the localized surface plasmon resonance with the copper (II) concentration, which effectively scales with the nanoparticle volume due to the origin of the absorption phenomenon, SHG relies on a surface origin of the response for sufficiently small nanoparticles. As a result, differences can be expected that could be potentially turned into advantages like improved Limit of Detection and shorter detection response time. The present study demonstrates that the SHG light scattered from aqueous suspensions of gold nanoparticles in the presence of copper (II) ions is indeed sensitive to the copper (II) ions concentration changes. A first approach based on intensity changes shows that there is a competition between the formation of corona-like structures centered around the gold nanoparticles due to the ionic interaction between copper (II) ions and the negatively charged citrate coated nanoparticles on one side, and, on the other side, aggregation of nanoparticles due to charge screening as the copper (II) bromide concentration increases. The former process dominates at low copper (II) concentrations whereas aggregation takes over above 1 mM copper (II) concentrations. A figure of merit is thus designed in order to provide a quantitative assessment of the sensing performance. In a further analysis, polarization resolved study of the SHG light scattered from the gold nanoparticles allows the determination of other figures of merit. The first one based on the depolarization ratio seems appropriate as it is based on the surface origin of the SHG response from gold nanoparticles whereas the second one, based on the retardation parameter, should not perform better than those derived from colorimetry methods.

INTRODUCTION

Detection of copper (II) ions is crucial in various fields, from medicine [1, 2] to food safety [3] and environment pollution. For example, the maximum allowed level of copper in drinking water has been set to about 20 μM [4]. However, due to significant copper (II) ion intake coming from, say, plumbing pipes, the recommended daily intake may be fulfilled from drinking water only [5]. Meanwhile, overdoses may lead to oxidative stress and interfere with the homeostasis of other elements, such as Ca, Fe or Mn [6]. Copper (II) homeostasis itself is responsible for pathologies associated with neurodegenerative diseases including Menkes and Wilson's disease, Alzheimer's or Parkinson's [7]. Consequently, a proposal for quick, simple and cost-efficient detection procedures should be of great help. An important class of sensing methods is based on optical phenomena, and more precisely, on changes in the optical properties of the sensing device in the presence of copper (II) ions [8]. A possibility is offered by gold nanoparticles (AuNPs) which exhibit a high sensitivity to surrounding medium changes [9], resulting in colorimetric sensing possibilities due to the shift of the Localized Surface Plasmon Resonance (LSPR) through either surrounding solvent changes or surface chemical binding [9]. Aggregation and de-aggregation of gold nanoparticles have also been proposed as the basis of copper (II) ions sensing. For example, after aggregation of polyvinylpyrrolidone (PVP)-stabilized AuNPs with 2-mercaptobenzimidazole (MBI), binding of copper (II) ions with MBI induces AuNPs redispersion [10]. Color changes, simply observed by the naked eye, indicated a 0.5 μM detection limit using UV-Visible spectroscopy. As opposed to de-aggregation, aggregation of citrate-stabilized AuNPs is induced with copper-citrate interaction [11]. In this case, a limit of detection of 5.0 mM was reported.

AuNPs colorimetric sensing methods are based on the change of AuNPs extinction, a linear optical phenomenon depending on the volume dependent absorption and scattering cross sections of AuNPs [12]. Hence, because the recognition step occurs at the AuNPs surface, faster methods with improved Limit of Detection (LoD) may be expected if based on surface dependent properties. This possibility is offered with some nonlinear optical phenomena that have consequently attracted attention. Second Harmonic Generation (SHG), the phenomenon where two photons at a fundamental frequency are converted into a single photon at the double frequency, is highly sensitive to centrosymmetry breaking and thus appears as a potential candidate for surface sensing [13].

In this report, Hyper Rayleigh Scattering (HRS), the incoherent scattering of SHG light, is investigated for aqueous suspension of 50 nm diameter AuNPs to assess the sensing potential towards copper (II) ions [14-16]. The study entails the use of the intensity and light polarization analysis of the scattered SHG intensity. Although the method in its details requires a close scrutiny of the nonlinear optical phenomenon, it appears that its setting up into a sensing method remains accessible for simple operation.

MATERIALS AND METHODS

50 nm diameter citrate-stabilized gold nanospheres as well as copper (II) bromide were purchased from Merck and used as received. Various concentrations of aqueous copper (II) bromide solutions were prepared using neat water (Millipore MilliQ 18 MΩ·cm). Addition of the

copper (II) bromide salt solutions to the gold nanospheres solutions was performed for different volumetric ratios. After 30 minutes, the HRS measurements were conducted.

UV-Visible spectra were recorded for all samples (Jasco, model V-730). The hydrodynamic diameter and zeta potential for all samples were determined by dynamic light scattering (DLS) (Malvern, model Zetasizer Nano ZS). The sample solution was illuminated with a 633 nm laser, and the light intensity scattered at an angle of 173° was measured. At least six consecutive measurements were carried out for each sample. The time-dependence autocorrelation function of the photocurrent was acquired every 10 s with 15 acquisitions for each measurement. The experimental AuNPs average diameter was determined with measurements at 25°C in water (viscosity 0.8872 mPa·s) using disposable folded capillary cells (DTS, model DTS1070). Electrophoretic mobilities were converted into zeta potential using Smoluchowski's formula [17]. DLS data were analyzed using DTS 8.02 software (Malvern Instruments).

The structure and morphology of the samples were studied using JEOL F-200 transmission electron microscope (JEOL Ltd., Tokyo, Japan) at an accelerating voltage of 80 kV. The 5 µL of the sample was placed on the copper grids with amorphous carbon, and next the sample was left until dry. The TVIPS camera (Germany) was used to determine the shape of the dispersed phase.

The HRS setup has been described elsewhere [18]. Briefly, the samples were excited by a femtosecond laser beam (Coherent, model Verdi X pumping a Mira 900) at fundamental wavelength of 800 nm with pulse length of 140 fs and 80 MHz repetition rate, that was gently focused with X10 objective in a configuration where excitation and collection directions are at

right-angle. The harmonic intensity was collected with a CCD camera connected to a spectrometer, preceded by a high bandpass filter. For polarization-resolved studies, the angle of polarization of the linearly polarized input beam was set with a half-wave plate and analyzed with a half-wave plate and a cube polarizer in order to preserve the detected polarization. The average input power was around 250 mW.

RESULTS AND DISCUSSION

AuNPs samples with Copper (II) bromide concentration ranging from 0 to 25 mM were prepared. Their UV-Visible spectra were then recorded, see Figure 1. The behavior of the extinction spectra can be described in terms of three phenomena: a red-shift of the LSPR peak, see Figure 2(a), where this peak located at 525 nm is attributed to the localized surface plasmon resonance (LSPR) of the individual 50 nm diameter AuNPs, a change of this peak amplitude, see Figure 2(b), and the appearance of a new band with a maximum around 780 nm, see Figure 2(c).

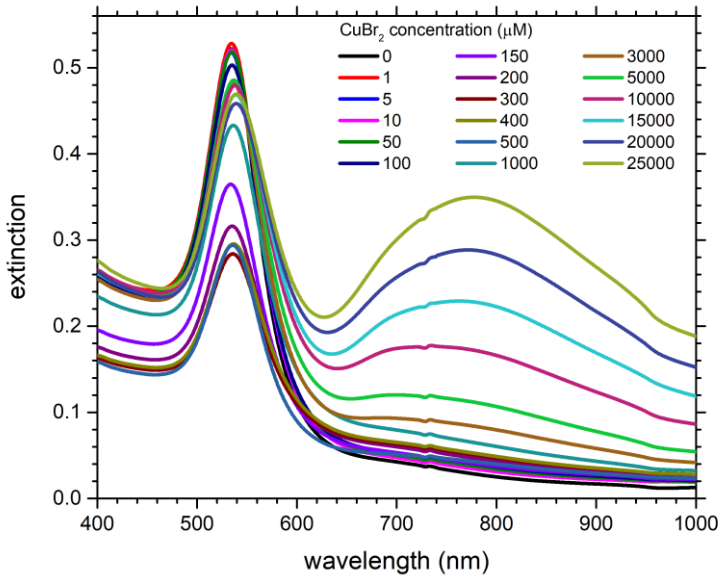

Figure 1: *UV-Visible extinction spectra of gold nanoparticles-copper (II) bromide mixtures. The color code is provided on the graph.*

The graphs exhibit two main regimes, the behavior being rather different below and above the 1 mM Copper (II) bromide limit. Below this concentration, the redshift of the band associated with the LSPR of individual AuNP evolves rapidly with Copper (II) bromide concentration. Above this limit, the increase continues but the dependence is not so rapid anymore. Meanwhile, the LSPR peak amplitude drops rapidly below the 1 mM Copper (II) bromide limit before stabilizing above this limit. Finally, the 780 nm extinction value also increases rapidly below the limit whereas it continues to increase with copper (II) bromide concentration but more slowly after the limit. Values shown in Figs. 2(a)-(c) are calculated from 5 separate measurements on different sample preparations, hence the relatively high uncertainties. From these UV-Visible extinction spectra, the following Figures of Merit (FoM) with respect to copper (II) bromide concentration

may be defined, namely $\Delta\lambda/\Delta c = 0.30 \pm 0.30$ nm·μM^{-1} and $(\Delta\lambda/\lambda)/\Delta c = (5.55 \pm 4.83) \times 10^{-4}\ \mu M^{-1}$ for a relative shift of the LSPR peak wavelength. Based on the relative extinction change for this same LSPR peak, one can define similarly $(\Delta A/A)/\Delta c = (5.10 \pm 5.13) \times 10^{-2}$ μM^{-1} and for the absorbance at 780 nm $(\Delta A/A)/\Delta c = (1.03 \pm 52.49) \times 10^{-2}\ \mu M^{-1}$. The uncertainty of the FoM based on the 780 nm is huge compared to the FoM value itself, a feature due to the very low extinction observed for low copper (II) bromide content, close to the detection limit of typical UV-Visible spectrometers. Similar features are observed for the LSPR peak-based FoM value which is lower or equal to its uncertainty. Only the relative change of the spectral position of the LSPR peak may thus be considered for sensing purposes at such small copper concentrations. In any case, considering the above FoM along their large uncertainties, and although linear optics based methods are much simpler to put up in practice, more appropriate methods are required, possibly based on more advanced optical processes.

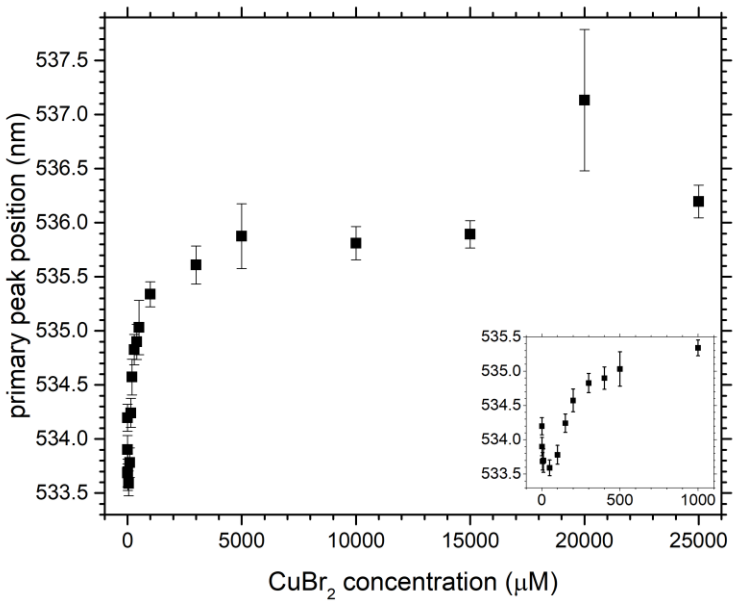

(a)

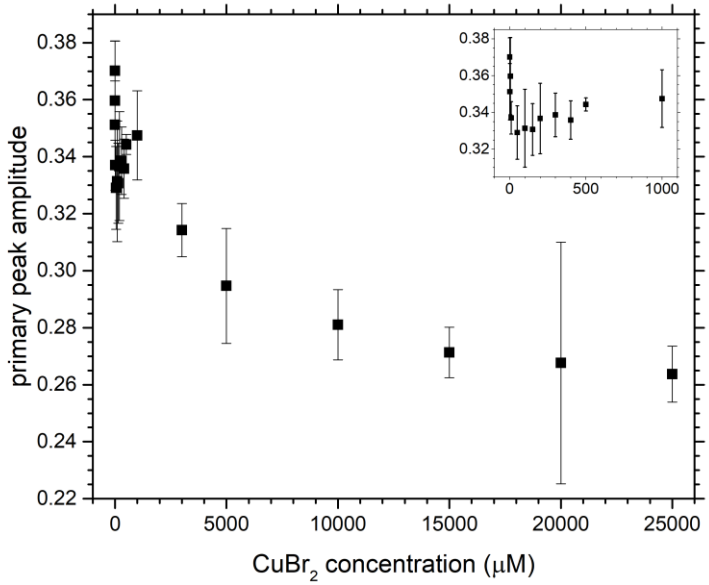
primary peak amplitude
CuBr2 concentration (μM)
0.22
0.24
0.26
0.28
0.30
0.32
0.34
0.36
0.38
0
5000
10000
15000
20000
25000
0.32
0.34
0.36
0.38
0
500
1000

(b)

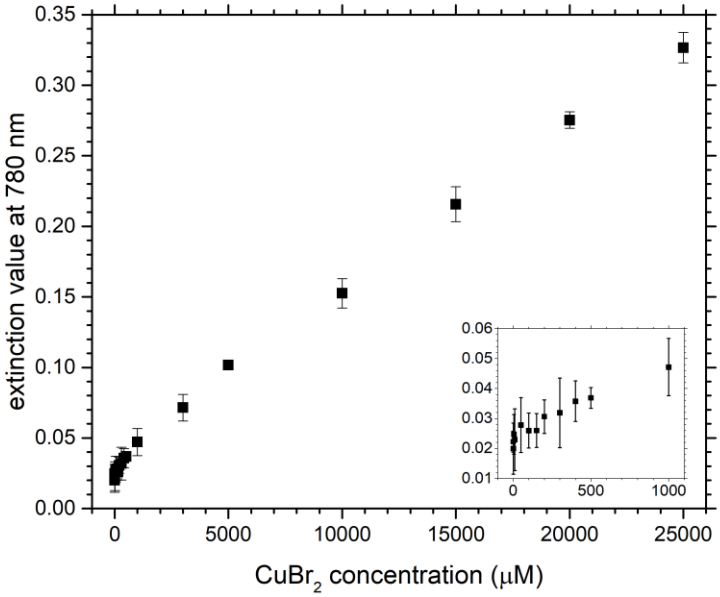
extinction value at 780 nm
CuBr2 concentration (μM)
0.00
0.05
0.10
0.15
0.20
0.25
0.30
0.35
0
5000
10000
15000
20000
25000
0.01
0.02
0.03
0.04
0.05
0.06
0
500
1000

(c)

Figure 2: *(a) Individual LSPR AuNP peak position and (b) amplitude as well as (c) extinction value at 780 nm derived from the UV-Visible spectra reported in Figure 1 as a function of the copper (II) bromide concentration. (Inserts) blow-up views at low concentrations.*

Complementary to the UV-Visible extinction spectra, Zeta potential, Dynamic Light Scattering (DLS) and Transmission Electronic Microscopy (TEM) measurements were performed, see Figures 3(a)-(b) and Figures S3(a)-(d) and S4(a)-(d). For samples with low Copper (II) bromide content, only minor changes in the hydrodynamic diameter are observed, with a small decrease, followed by a steady increase above this limit. For the Zeta potential, a rapid increase is observed before a plateau is reached after the 1 mM Copper (II) bromide limit.

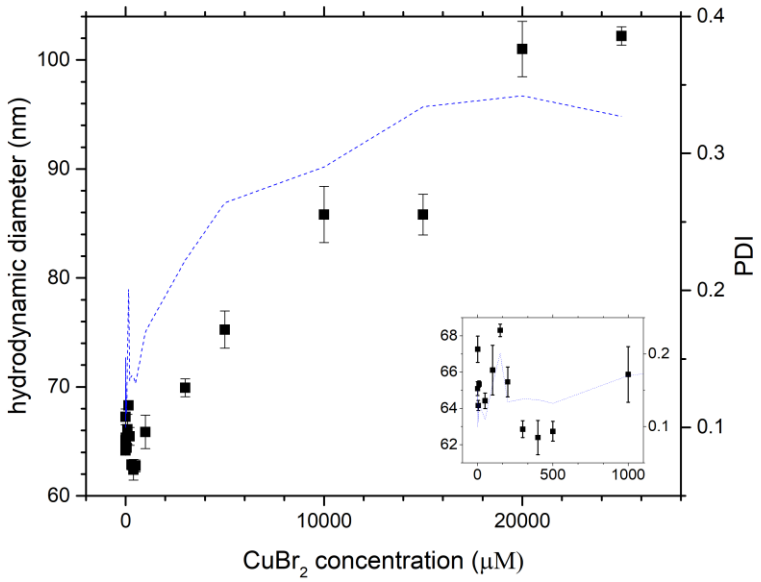

(a)

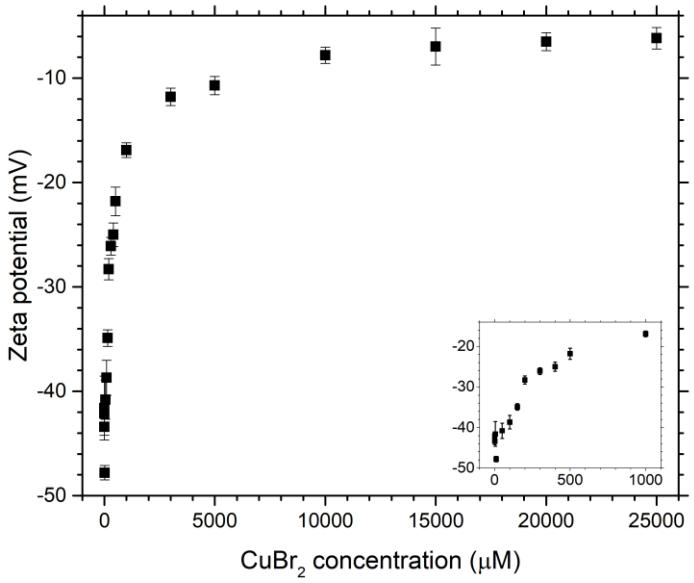

(b)

Figure 3: *(a) Hydrodynamic diameter along with the Polydispersity Index (PDI) (blue dashed line) and (b) Zeta potential of the studied samples as a function of the copper (II) bromide concentration. (Inserts) blow-up views at low concentrations.*

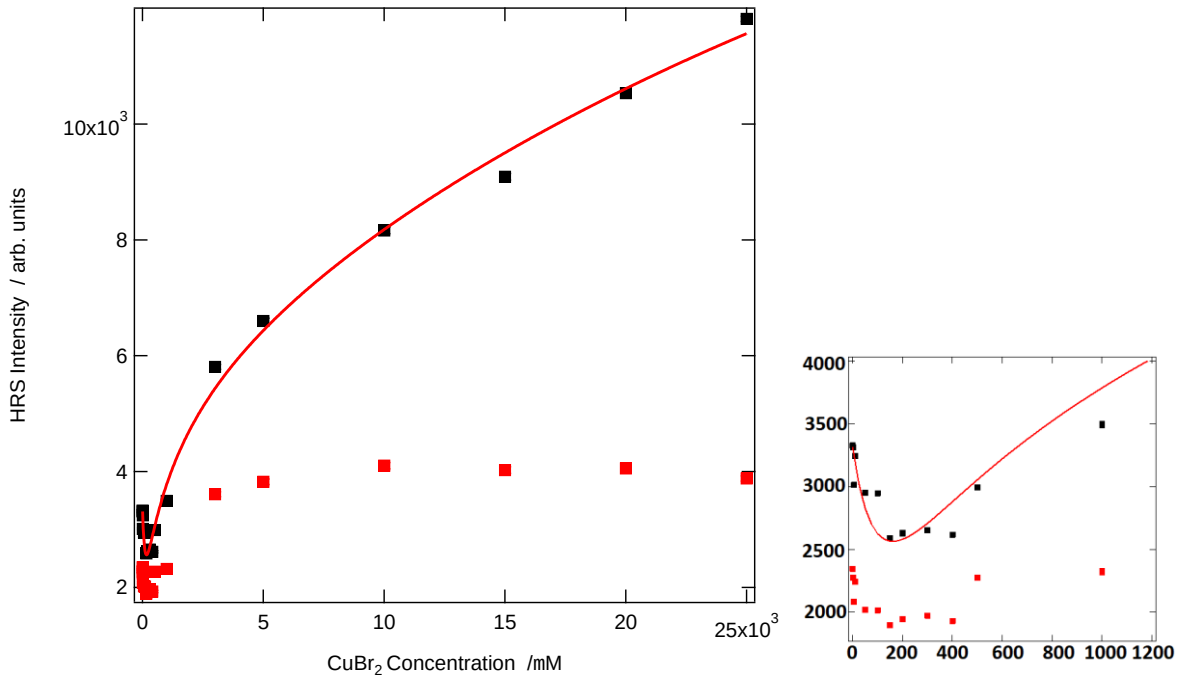

(main) (insert)

Figure 4: *(main) Hyper Rayleigh Scattering (HRS) intensity as a function of copper (II) bromide concentration, (red squares) HRS intensity uncorrected for self-extinction, (black squares) HRS intensity corrected for self-extinction, (red line) adjustment with the model, see text, (insert) blow up view of the same graph at low concentrations.*

All these observations may be rationalized with two main processes: a weak interaction between copper (II) ions and citrate dominating below the 1 mM copper (II) bromide limit followed by AuNPs aggregation dominating above this limit. The redshift of the primary extinction peak is probably caused by the formation of positively charged copper (II) ions corona-like structures around the negatively charged citrate capped AuNPs [19]. This ionic interaction may be responsible for a weak shrinkage of the hydrodynamic diameter observed in Figure 3(a) at low

copper (II) bromide concentrations. This ionic association between copper (II) ions and citrate has already been reported in the literature at low copper concentrations below 30 μM [19]. The possibility that the citrate anions would be replaced to some extent by bromide anions would not modify the formation of the copper (II) ions corona as the latter likely stems from electrostatic interactions. Note nevertheless that a change of bromide for chloride provides a similar response, see Figure S1. On the opposite, AuNPs aggregation is known to occur at copper concentrations above 1 mM [11]. In fact, the two processes of weak ionic interactions and aggregation occur simultaneously. Below 1 mM, weak ionic interactions dominate leading to a weak decrease of the hydrodynamic diameter with rapid changes in the Zeta potential. When aggregation dominates, as indicated by the steady increase of the hydrodynamic diameter, the Zeta potential reaches a plateau value. Moreover, the increase of the Polydispersity Index is in line with appearance of aggregates, the size distribution of which is typically rather large.

Hyper Rayleigh Scattering experiments at 800 nm excitation were thus conducted on the described above samples, see Figure 4. The process of HRS is highly sensitive to the nanoparticle surface changes, and therefore to the changes of the immediate surrounding of the nanoparticles and indeed the HRS intensity lowers immediately with small copper (II) bromide additions. Nevertheless, at a concentration of about 400 μM, the HRS intensity starts to rise steadily. Interestingly, the absorbance maximum recorded at 780 nm, close to 800 nm which is the fundamental wavelength of the measurements, remains extremely weak at low copper content below about 400 μM, corresponding to an extinction below 0.05, see Figure 1. It must be however noted, that the appearance of the peak around 780 nm is associated also with the appearance of copper (II) bromide, see Figure S2 (a) in the Supporting Information File.

However, taking into consideration Figure S2 (b) with subtracted copper (II) bromide influence, the tendency remains similar. An important factor that significantly affects the HRS behaviour at higher copper contents is re-absorption, see Figure 4 where the uncorrected and extinction corrected HRS intensities as a function of copper (II) bromide concentration are provided. The correction for self-extinction was obtained using the following expression :

$$I_{HRS} = I_{0,HRS} \cdot 10^{(2A_{800}+A_{400})/2} \quad (1)$$

where I_{HRS} is the corrected HRS intensity, $I_{0,HRS}$ stands for HRS intensity before correction, A_{800} and A_{400} are extinction values at 800 nm and 400 nm respectively. The factor $1/2$ is introduced to account for the difference in the path length between UV-visible extinction and HRS measurements. The extinction corrected HRS intensity was then modeled using a simple model involving the first hyperpolarizability tensor $\boldsymbol{\beta}_m$ for the gold nanoparticles and $\boldsymbol{\beta}_d$ for the nanoparticle dimers. The total HRS intensity has the expression :

$$I_{HRS} = G[N_m\langle\beta_m^2\rangle + N_d\langle\beta_d^2\rangle] \quad (2)$$

where N_i stands for the monomer and dimer concentrations and the $\langle \quad \rangle$ bracket for orientational averaging. G is a general constant. It is important to underline here that the model is simplified to a unique monomer – dimer equilibrium whereas it is possible to introduce larger aggregates.

However, introducing the possibility to have the formation of larger aggregates involving three or more gold nanoparticles would only bring further complexity in the model with new but unnecessary parameters. The first hyperpolarizabilities were of the form :

$$\boldsymbol{\beta}_i = \boldsymbol{\beta}_{i0} + \boldsymbol{\Delta\beta} exp[-\alpha_i C] \quad (3)$$

where $\boldsymbol{\beta}_i$ is the first hyperpolarizability of the monomer or dimer with $i = m, d$, $\boldsymbol{\beta}_{i0}$ the first hyperpolarizability of the monomer or dimer at large copper (II) ion concentration, $\boldsymbol{\Delta\beta}$ the change in first hyperpolarizability due to copper (II) ion concentration and α_i the scaling parameter determining the first hyperpolarizability dependence with copper (II) ions concentration C. Bold characters are used to indicate tensors, Eq.(3) applying for any tensor element whereas non bold characters are used in Eq.(2) because tensor elements are selected by the polarization configuration. Finally, the monomer – dimer equilibrium is defined through an equilibrium constant itself dependent on the copper (II) ion concentration. Adjustment of the model to the experimental data is given in Figure 4, providing a correct description of the behavior of the HRS intensity as a function of the copper (II) ion concentration. This simple model, once linearized at very low copper (II) ion concentration, provided the following FoM defined as the relative HRS intensity change as a function of copper (II) ion concentration, namely $[(\Delta I_{HRS}/I_{HRS})/C]_{C=0} = -(5 \pm 2) \times 10^{-3}$ μM^{-1}. Note that this FoM is negative due to the initial HRS intensity decrease and that it may be preferable to redefine it as its absolute value and hence report this FoM as $[|\Delta I_{HRS}/I_{HRS}|/C]_{C=0} = (5 \pm 2) \times 10^{-3}$ μM^{-1}. The concentration range over which that FoM was determined is however limited to the 0 – 150 μM range. This

resulting FoM provides a LoD well below 1 mM, reaching about 100 µM with possibilities of improvement by lengthening the acquisition time.

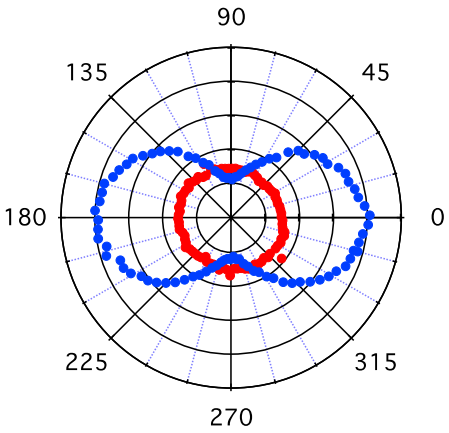

Figure 5 : *Polar plot of the polarization-resolved normalized HRS intensity as a function of the angle of polarization of the fundamental beam, (blue) vertically polarized HRS intensity, (red) horizontally polarized HRS intensity. The presented result is of pure nanoparticles, i.e. without copper (II) bromide. Remaining polar plots can be found in the Supporting Information file, Figure S5 (a) – (h).*

To further investigate the sensing potential of the method, polarization-resolved measurements were performed as a function of copper (II) bromide concentration. The resulting experimental data, gathered in Figure 5 (sample without copper (II) bromide) and Supplementary Information file (see Figures S5 (a)-(h) for the remaining samples), were fitted with the following expression [20] :

$$I_{HRS}^{X} = a^{X}cos^{4}\gamma + b^{X}cos^{2}\gamma\, sin^{2}\gamma + c^{X}sin^{4}\gamma \quad (4)$$

where I_{HRS}^{X} indicates polarization resolved HRS intensity, a^{X}, b^{X} and c^{X} are polarized intensity parameters and X stands for either vertically (V) or horizontally (H) polarized output harmonic intensity and γ is the angle of polarization of the linearly polarized fundamental beam. In order to provide a deep insight into the response, three parameters were further computed :

$$D^{V} = c^{V}/a^{V} \quad (5a)$$

$$\zeta^{V} = (b^{V} - a^{V} - c^{V})/b^{V} \quad (5b)$$

$$\zeta^{H} = (a^{H} - c^{H})/(a^{H} + c^{H}) \quad (5c)$$

where D^{V} is the depolarization ratio [18] and ζ^{V} and ζ^{H} are the so-called retardation parameters [20, 21]. All these three parameters are auto-normalized as they result from ratios of the HRS intensity collected for specific fundamental and harmonic angles of polarization. The depolarization ratio D^{V} provides insight into the symmetry of the nonlinear response within the irreducible susceptibility spherical tensor description, with a value ranging from 1/9 for a pure dipolar symmetry to 2/3 for an octupolar symmetry within Kleinmann approximation. The retardation parameters ζ^{V} and ζ^{H} are related to size through the phase retardation occurring within the nanoparticles. Hence, they vanish for small nanoparticles, i.e. for sizes below about 40 nm in the case of gold nanoparticles and can reach about unity for the largest spherical nanoparticles, beyond 150 nm diameter or so. The depolarization ratio D^{V} increases with the copper (II) bromide concentration from an initial value of about 0.3, a standard value for gold

nanoparticles, before reaching a plateau value of about 0.46 at a concentration of 5 mM, see Figure 6(a). This value in the range between 0.3 and 0.4 indicates a similar contribution from dipolar and octupolar irreducible tensor contributions [22]. This parameter increase from 0.3 up to 0.44 indicates that the presence of copper (II) corona-like structures established around the nanoparticles favors the octupolar response against the dipolar one. This may be explained through corona-like structures somehow passivating the initial surface response of the nanoparticle and leading to a nonlinearity better distributed around the nanoparticle surface, still in a non-centrosymmetric manner [23]. At higher copper (II) concentrations, this depolarization ratio reaches a plateau value determined by the nanoparticle aggregates. Their geometry therefore favors a nonlinearity with an octupolar symmetry, probably due to the random spatial arrangement of the gold nanoparticles within the aggregates.

The retardation parameter ζ^V retains a non vanishing value in the absence of copper (II) ions already for 50 nm diameter gold nanoparticles, in agreement with literature [24]. The second retardation parameter ζ^H retains a non vanishing value, too, but the latter is rather small and then further decreases towards a vanishing value at the highest copper (II) concentrations. Their behavior is thus contrasted. Indeed, to the contrary, the ζ^V parameter exhibits a strong increase followed by a rapid decrease and then a plateau value when aggregation takes place as the copper (II) concentration increases. The ζ^V parameter presents a more reliable behavior with copper (II) bromide additions due to its larger value [20, 24]. In the regime of low concentrations, as copper (II) ions form corona-like structures around the AuNPs, its rapid increase may relate to some extent to the weakening of the non-centrosymmetry of the gold nanoparticles due to a weakening

of the surface contribution. However, it is interesting to note that, when the aggregation takes place, the parameter ζ^V quickly stabilizes [22, 23, 25].

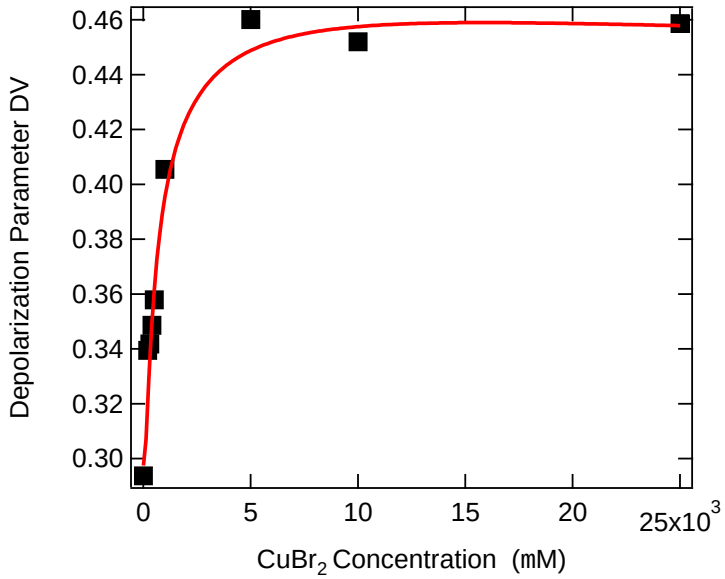

(a)

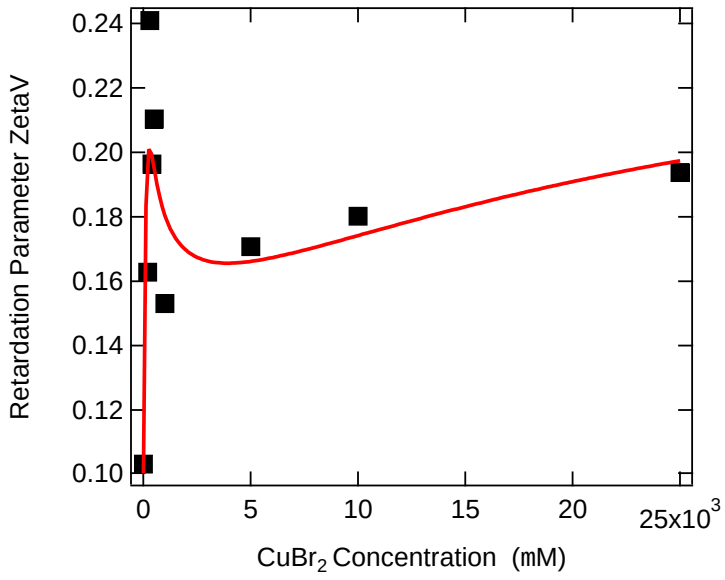

(b)

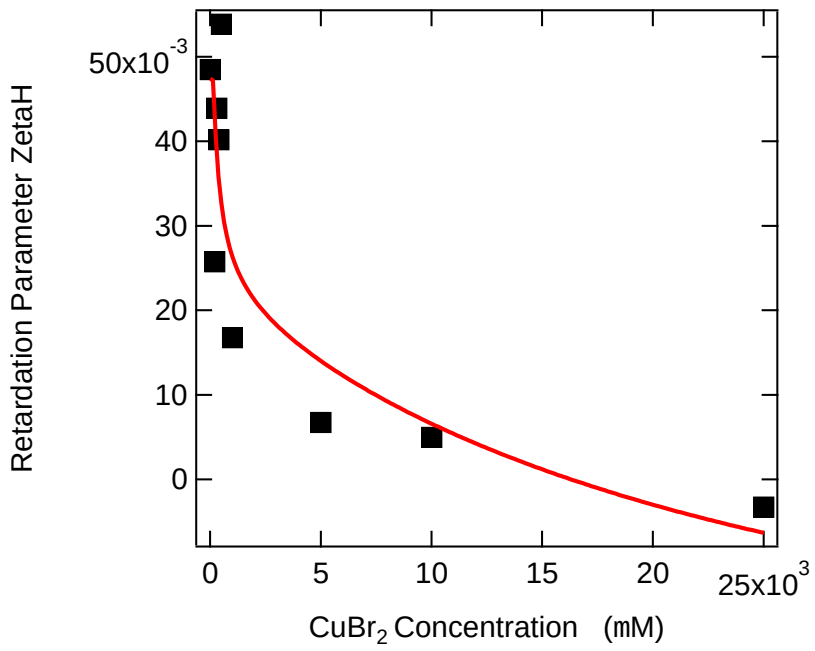

(c)

Figure 6 : *(a) Depolarization ratio D^V and retardation parameters (b) ζ^V and (c) ζ^H with respect to copper (II) bromide concentration.*

Because of its rather low value, the ζ^H parameter does not probably constitute a good FoM. It also switches from positive to negative values at large copper (II) ion concentration and this is related to the dominating dimer hyperpolarizability over that of the monomers in this concentration region. All parameters resulting from the adjustment are reported in Table S1 in the Supplementary Information file.

In order to quantitatively assess the LoD of the method, figures of merit can be derived. From intensity measurements, one can simply derive as a figure of merit the ratio between the relative HRS intensity change $\Delta I_{HRS}/I_{HRS}$ with respect to the concentration change C, see above. If polarization resolved intensities are now used, then other figures of merit can be formed with the depolarization ration D^V or the first retardation parameter ζ^V. Such FoM expressed as $[(\Delta D^V/D^V)/C]_{C=0}$ or $[(\Delta \zeta^V/\zeta^V)/C]_{C=0}$ may then be built either from the model or directly from the experimental data with a linear adjustment at the origin. Both lead to similar values. Then, FoMs of the order of 1×10^{-4} μM^{-1} are obtained. To our knowledge, no similar FoM have been proposed in the literature yet, as such figures of merit are rather unusual. It must be pointed out though that the $[(\Delta \zeta^V/\zeta^V)/C]_{C=0}$ figure of merit is based on retardation and therefore scales with the gold nanoparticle diameter, or size. Hence, this figure of merit should not be competitive as compared to colorimetry based sensing methods similarly based on size scaling as well. Hence, using larger diameter gold nanoparticles as compared to the present 50 nm diameter ones should not bring any improved LoD. On the opposite, the $[(\Delta D^V/D^V)/C]_{C=0}$ figure of merit, built from the polarization plots and the a^V and c^V parameters the origin of which is surface specific, fulfills the initial demand of a surface specific FoM with an improved value as compared to the HRS intensity based FoM $[[\Delta I_{HRS}/I_{HRS}]/C]_{C=0}$. Note though, that in principle, the $[(\Delta D^V/D^V)/C]_{C=0}$ FoM requires twice as many measurements due to the HRS intensity ratio nature of the D^V parameter.

CONCLUSIONS

In this study, the potential of a sensing method based on the nonlinear optical process of SHG using gold nanoparticles is investigated. In addition to standard control based on UV-visible extinction spectroscopy, Zeta potential and DLS measurements, an intensity and polarization based study of the changes of the HRS response with the copper (II) bromide concentration is performed. It appears that a competition between the formation of copper (II) induced corona-like structures centered around the gold nanoparticles and the aggregation of the latter is taking place. The former process appears at low copper (II) bromide concentrations, well below 1 mM, whereas aggregation takes over above this limit. The HRS intensity analysis exhibits first an intensity decrease at low copper (II) bromide concentration due to the corona-like structures formation followed by an increase as aggregation takes place. Saturation of the intensity then occurs at the largest copper (II) bromide concentrations precluding the use of HRS as a sensing method in this concentration range. Likewise, the polarization-resolved HRS analysis reveals a similar retardation behaviour at high copper (II) bromide concentration for both the depolarization and the retardation parameters. Hence, at low concentrations, the HRS based method appears to present a useful approach for copper (II) sensing with the highest Figure of Merit in the range of $(5 \pm 2) \times 10^{-3}$ μM^{-1} in the 0 – 150 μM $CuBr_2$ range, a clearly improved magnitude as compared to UV-Visible extinction spectroscopy methods based on the relative spectral localisation of the LSPR peak. In fact, as shown initially for comparison, the UV-Visible spectroscopy measurement of the LSPR shift turns out to be unreliable for this copper (II) ions sensing experiment as the uncertainty is very close to the obtained value.

In the case of polarization measurements, FoM based on the retardation parameter ζ^V that is non zero for relatively large diameter gold nanoparticles due to a size scaling, suggests that the figure of merit should not be better than those derived from colorimetry methods where the same scaling operates. On the opposite, a FoM of the form $[(\Delta D^V/D^V)/C]_{C=0}$ presents advantages with an improved value of the order of 1×10^{-4} μM^{-1}. On a final note, it is pointed out first that the nonlinear dependence of these two FoMs with copper (II) bromide concentration may bring a further degree of complexity for the establishment of a sensing method preferably based on linear dependencies, unless linearization is introduced at low copper (II) concentrations. Second, there remains the question of the selectivity and interference of the copper (II) ions sensing in the case of waters containing other ions. In this work, the origin of the interaction between copper (II) ions and the negatively charged gold nanoparticles is of likely electrostatic origin. Hence, selectivity may not be achieved and interference may occur with other ions. These two aspects will be investigated in further studies.

SUPPORTING INFORMATION.

Complementary data for UV-visible extinction spectroscopy, TEM, complete list of the adjusted parameters of the model, and polarization resolved HRS intensity plots of the studied samples.

ACKNOWLEDGEMENTS

K.N. and K.M. acknowledge funding from the National Science Centre in Poland within the Harmonia DEC/2016/22/M/ST4/00275 project and funding from the National Science Centre in Poland within the Opus UMO-2019/35/B/ST4/03280 project. All authors acknowledge funding

from the PPN/BFT/2019/1/00030/U/0001 PHC POLONIUM project, cofunded by the Polish National Agency For Academic Exchange and Campus France.

REFERENCES

1. Desai V.; S. G. Kaler S. G. Role of copper in human neurological disorders. *The Am. J. Clin. Nutr.* **2008**, *88*, 855S-858S.
2. Lutsenko S.;Barnes N. L.; Bartee M. Y.; Dmitriev O. Y. Function and Regulation of Human Copper-Transporting ATPases. *Physiol. Rev.* **2007,** *87,* 1011-1046.
3. Xiang G.; Wen S.; Jiang X.; Liu X.; He L. Determination of Trace Copper(II) in Food Samples by Flame Atomic Absorption Spectrometry after Cloud Point Extraction. Iran. J. Chem. Chem. Eng. **2011**, *30*, 101-107.
4. Liu J.; Lu Y.; A DNAzyme Catalytic Beacon Sensor for Paramagnetic Cu^{2+} Ions in Aqueous Solution with High Sensitivity and Selectivity. *J. Am. Chem. Soc.* **2007**, *129*, 9838-9839.
5. Wu M.; Zhi M.; Liu Y.; Han J.; Qin Y. In situ analysis of copper speciation during in vitro digestion: Differences between copper in drinking water and food. *Food Chem.*, **2022**, *371*.
6. Witt B.; Stiboller M.; Raschke S.; Friese S.; Ebert F.; Schwerdtle T. Characterizing effects of excess copper levels in a human astrocytic cell line with focus on oxidative stress markers. *J. Trace Elem. Med. Biol.* **2021**, *65*.
7. Scheiber I.F.; Mercer J. F. B.; Dringen R. Metabolism and functions of copper in brain. *Prog. Neurobiol.* **2014,** *116*, 33-57.
8. Udhayakumari D.; Naha S.; Velmathi S. Colorimetric and fluorescent chemosensors for Cu^{2+}. A comprehensive review from the years 2013-15. *Anal. Methods* **2017**, *9*, 552-578.
9. Hu M.; Novo C.; Funston A.; Wang H.; Staleva H.; Zou S.; Mulvaney P.; Xia Y.; Hartland G. V. Dark-field microscopy studies of single metal nanoparticles:

understanding the factos that influence the linewidth of the localized surface plasmon resonance. *J. Mater. Chem.* **2008,** *18*, 1949-1960.

10. Ye Y.; Lv M.; Zhang X.; Zhang Y. Colorimetric determination of copper(II) ions using gold nanoparticles as a probe. *RSC Adv*. **2015**, *5*, 102311-102317.
11. Salcedo A. R. M.; Sevilla III F. B. Citrate-Capped Gold Nanoparticles as Colorimetric Reagent for Copper (II) Ions. *Philipp. Sci. Lett.* **2013**, *6*, 90-96.
12. Bohren C.F.; Huffman D. R. *Absorption and Scattering of Light by Small Particles*; John Wiley & Sons Inc.: New York, NY, USA, 1983.
13. Tran R. J.; Sly K. L.; Conboy J. C. Applications of Surface Second Harmonic Generation in Biological Sensing. *Annu. Rev. Anal. Chem.* **2017**, *10*, 387-414.
14. Hao E. C.; Schatz G. C.; Johnson R. C.; Hupp J.T. Hyper-Rayleigh scattering from silver nanoparticles. *J. Chem. Phys.* **2002**, *117*, 5963.
15. Nadolski K.; Benichou E.; Tarnowicz-Staniak N.; Żak A.; Jonin C.; Matczyszyn K.; Brevet P-F. Adverse Role of Shape and Size in Second-Harmonic Scattering from Gold Nanoprisms.*J. Phys. Chem. C* **2020**, *124*, 14797-14803.
16. Ngo H. M.; Lai N. D.; Ledoux-Rak I. High second-order nonlinear response of platinum nanoflowers: the role of surface corrugation. *Nanoscale* **2016**, *8*, 3489-3495.
17. Sze A.; Erickson D.; Ren L.; Li D. Zeta-potential measurement using the Smoluchowski equation and the slope of the current–time relationship in electroosmotic flow. *J. Colloid Interface Sci.* **2003**, *261*, 402-410.
18. Nappa J.; Revillod G.; Russier-Antoine I.; Benichou E.; Jonin C.; Brevet P-F. Electric dipole origin of the second harmonic generation of small metallic particles. *Phys. Rev. B* **2005**, *71*, 165407.

19. Wang N.; Dai H.; Sai L.; Ma H.; Lin M. Cooper ion-assisted gold nanoparticle aggregates for electrochemical signal amplification of lipopolysaccharide sensing. *Biosens. Bioelectron.* **2019**, *126*, 529-534.

20. Butet J.; Bachelier G.; Russier-Antoine I.; Jonin C.; Benichou E.; Brevet P-F., Interference between Selected Dipoles and Octupoles in the Optical Second-Harmonic Generation from Spherical Gold Nanoparticles. *Phys. Rev. Lett.* **2010**, *105*, 077401.

21. El Harfouch Y.; Benichou E.; Bertorelle F.; Russier-Antoine I.; Jonin C.; Lascoux N.; Brevet P-F. Hyper-Rayleigh Scattering from Gold Nanorods.*J. Phys. Chem. C* **2014**, *118*, 609-616.

22. Brasselet S.; Zyss J. Multipolar molecules and multipolar fields: probing and controlling the tensorial nature of nonlinear molecular media. *J. Opt. Soc. Am. B* **1998**, *15*, 257-288.

23. Duboisset J.; Brevet P-F., Second-Harmonic Scattering-Defined Topological Classes for Nano-Objects. *J. Phys. Chem. C* **2019,** *123*, 25303-25308.

24. Russier-Antoine I.; Benichou E.; Bachelier G.; Jonin C.; Brevet P-F., Multipolar Contributions of the Second Harmonic Generation from Silver and Gold Nanoparticles. *J. Phys. Chem. C* **2007**, *111*, 9044-9048.

25. Bachelier G.; Russier-Antoine I.; Benichou E.; Jonin C.; Brevet P-F. Multipolar second-harmonic generation in noble metal nanoparticles.*J. Opt. Soc. Am. B* **2008**, *25*, 955-960.

26. Park J.-W.; Shumaker-Parry S. Structural Study of Citrate Layers on Gold Nanoparticles: Role of Intermolecular Interactions in Stabilizing Nanoparticles. *J. Am. Chem. Soc.* **2014**, *136*, 1907-1921.

TOC Graphic